Presenilins are essential for regulating neurotransmitter release

Published in final edited form as:
Nature. 2009 July 30; 460(7255): 632–636. doi:10.1038/nature08177.

Presenilins are Essential for Regulating Neurotransmitter Release

Chen Zhang[1,2], **Bei Wu**[1], **Vassilios Beglopoulos**[1], **Mary Wines-Samuelson**[1], **Dawei Zhang**[1], **Ioannis Dragatsis**[3], **Thomas C. Südhof**[2], and **Jie Shen**[1]

[1]Center for Neurologic Diseases, Brigham & Women's Hospital, Program in Neuroscience, Harvard Medical School, Boston, MA, 02115, USA

[2]Department of Molecular and Cellular Physiology, Howard Hughes Medical Institute, Stanford University School of Medicine, Palo Alto, CA 94304, USA

[3]Department of Physiology, The University of Tennessee, Health Science Center, Memphis, TN 38163, USA

Summary

Mutations in the *presenilin* genes are the major cause of familial Alzheimer's disease (AD). Loss of presenilin activity and/or accumulation of amyloid-β peptides have been proposed to mediate the pathogenesis of AD by impairing synaptic function1¯5. However, the precise site and nature of the synaptic dysfunction remain unknown. Here we employ a genetic approach to inactivate presenilins conditionally in either presynaptic (CA3) or postsynaptic (CA1) neurons of the hippocampal Schaeffer-collateral pathway. We found that long-term potentiation (LTP) induced by theta burst stimulation is decreased after presynaptic but not postsynaptic deletion of presenilins. Moreover, presynaptic but not postsynaptic inactivation of presenilins alters short-term plasticity and synaptic facilitation. The probability of evoked glutamate release, measured with the open-channel NMDA receptor antagonist MK-801, is reduced by presynaptic inactivation of presenilins. Strikingly, depletion of endoplasmic reticulum Ca^{2+}-stores by thapsigargin or blockade of Ca^{2+}-release from these stores by ryanodine receptor inhibitors mimics and occludes the effects of presynaptic presenilin inactivation. Collectively, these results reveal a selective role for presenilins in the activity-dependent regulation of neurotransmitter release and LTP induction via modulation of intracellular Ca^{2+}-release in presynaptic terminals, and further suggest that presynaptic dysfunction might be an early pathogenic event leading to dementia and neurodegeneration in AD.

Conditional inactivation of presenilins in excitatory neurons of the mouse postnatal forebrain causes synaptic dysfunction, memory impairment and age-dependent neurodegeneration3›6. Prior to the onset of neurodegeneration, paired-pulse facilitation, long-term potentiation and NMDA receptor-mediated responses are altered3, suggesting that synaptic defects caused by loss of presenilins may be a cellular precursor of neuronal cell death. To determine the precise synaptic site of presenilin function, we performed a systematic genetic analysis through the restriction of presenilin inactivation to hippocampal CA1 or CA3 neurons. This strategy permitted selective examination of the effects of

*Corresponding author: Jie Shen, Center for Neurologic Diseases, Harvard Medical School, New Research Building, Rm 636E, 77 Avenue Louis Pasteur, Boston, MA 02115. Tel: 617 525 5561, Fax: 617 525 5522, jshen@rics.bwh.harvard.edu.
Author contributions CZ, BW, VB and MWS performed experiments and contributed to figures; DZ performed experiments; ID provided reagents; CZ, TCS and JS designed the research and wrote the paper.
Author information The authors declare no conflict of interest. Correspondence and requests for materials should be addressed to J.S. (jshen@rics.bwh.harvard.edu).

presenilin inactivation in either presynaptic or postsynaptic neurons of the Schaeffer-collateral pathway.

We crossed *fPS1/fPS1; PS2-/-* mice to *Camk2a-Cre*7 and *KA1-Cre*8 transgenic mice to produce CA1- and CA3-restricted *presenilin* conditional double knockout (*PS* cDKO) mice. *In situ* hybridization confirmed the selective loss of *PS1* expression in CA1 and CA3 neurons of CA1- and CA3- *PS* cDKO mice, respectively, at 2 months of age (Fig. 1a). We also crossed *Camk2a-Cre* and *KA1-Cre* mice to *Rosa26-lacZ* reporter transgenic mice, and observed the expected patterns of CA1- and CA3-restricted β-galactosidase expression (Fig. 1b).

We next examined the effect of selective *PS* inactivation in CA1 or CA3 neurons on theta-burst stimulation (TBS)-induced long-term potentiation (LTP), which is impaired in *PS* cDKO mice lacking PS in both CA3 and CA1 neurons3. Surprisingly, TBS-induced LTP is normal in CA1-*PS* cDKO mice but is markedly impaired in CA3-*PS* cDKO mice (Fig. 1c). Thus, presynaptic but not postsynaptic PS are required for TBS-induced LTP. To determine whether postsynaptic NMDA receptor (NMDAR)-mediated responses are affected in these mutant mice, we measured AMPA receptor- (AMPAR-) and NMDAR-dependent synaptic responses but detected no change in the NMDAR/AMPAR ratio in CA3- or CA1-*PS* cDKO mice (Fig. 1d). Moreover, input/output curves of NMDAR-dependent responses are normal in CA3- or CA1- *PS* cDKO mice (Fig. 1e). Thus, loss of PS in either presynaptic or postsynaptic neurons alone is insufficient to impair NMDAR-mediated responses. Similarly, input-output coupling (Supplementary Fig. 1) and current-voltage (I-V) relationship (Supplementary Fig. 2) of AMPAR-mediated synaptic responses are normal in CA3-*PS* cDKO mice. These results demonstrate that LTP deficits caused by presynaptic *PS* inactivation are not due to impaired postsynaptic receptor-mediated responses.

We thus investigated whether presynaptic activity is impaired during LTP induction, which could account for the observed LTP deficit. Indeed, we found that short-term depression during the initial stimulus train of TBS is increased in CA3-*PS* cDKO mice (Fig. 2a). Paired-pulse facilitation (PPF) and synaptic frequency facilitation are reduced in CA3-*PS* cDKO mice but normal in CA1-*PS* cDKO mice (Fig. 2b, 2c), which are confirmed by whole-cell recordings (Supplementary Figs. 3, 4). Moreover, the deficit in synaptic facilitation in CA3-*PS* cDKO mice is calcium-dependent and is rescued by higher external Ca^{2+} concentrations (Fig. 2d, Supplementary Fig. 5). Consistent with previous reports3,9, inactivation of PS1 or PS2 alone is insufficient to alter frequency facilitation or PPF (Supplementary Figs. 6, 7). The replenishment of the readily-releasable pool after depletion is also normal in CA3-*PS* cDKO mice (Supplementary Fig. 8), arguing against an impairment of synaptic vesicle recycling as a cause of the decreased synaptic facilitation.

To test directly whether presynaptic inactivation of presenilins alters the probability of glutamate release, we measured the overall release probability using the open channel blocker MK-801, which irreversibly blocks NMDARs upon each synaptic release event10,11. Thus, during low-frequency stimulation in the presence of MK-801 and of AMPAR blockade, the rate at which NMDAR-mediated synaptic responses declines reflects the average release probability of the synapses. We found that the decay rate of postsynaptic responses as a function of stimulus number is decreased in CA3-*PS* cDKO mice (Fig. 3a). When these results were fitted to a single exponential as a rough measure of the average release probability, we observed an almost 2-fold increase in the decay constant in CA3-*PS* cDKO mice (Fig. 3b). This result reveals a major decrease in release probability in CA3-*PS* cDKO mice, demonstrating a critical role for presenilins in regulating the probability of glutamate release. Spontaneous miniature EPSCs, however, are normal in frequency and

amplitude in CA3-*PS* cDKO mice (Supplementary Fig. 9), suggesting that a defect in Ca^{2+}-dependent release may account for the observed presynaptic phenotypes.

Evoked neurotransmitter release is dependent upon the local elevation of intracellular calcium concentrations. Presynaptic Ca^{2+} increases are caused by Ca^{2+} influx via voltage-gated calcium channels (VGCCs) and by calcium release from intracellular stores12. Since changes in Ca^{2+} influx via VGCCs have been reported to affect release probability10,11, we measured VGCC currents in the somata of CA3 neurons and found unaltered I-V relationship in CA3-*PS* cDKO mice (Supplementary Fig. 10). Thus, the change in release probability in CA3-*PS* cDKO mice is unlikely due to VGCC dysfunction. Since presenilins have been reported to be involved in the regulation of Ca^{2+} homeostasis in intracellular stores13-16, we examined the effect of depletion of intracellular Ca^{2+} stores on synaptic facilitation in CA3-*PS* cDKO mice. Thapsigargin, which irreversibly blocks Ca^{2+} pumps on the endoplasmic reticulum (ER), thereby abolishing intracellular Ca^{2+} release17, suppresses synaptic facilitation during high-frequency stimulation in control synapses, but has no discernable effect in presenilin-deficient nerve terminals (Fig. 3c). Thus, thapsigargin treatment mimics and occludes the effect of *PS* inactivation on synaptic facilitation, suggesting that dysregulation of intracellular Ca^{2+} release underlies the presynaptic defects in CA3-*PS* cDKO mice.

Calcium release from the ER is mediated through two major types of receptors: ryanodine receptors (RyRs), which mediate calcium-induced calcium release (CICR), and inositol 1,4,5-triphosphate receptors (IP_3Rs). We therefore tested the effect of specific inhibitors for RyRs or IP_3Rs on synaptic facilitation18-20. Blockade of RyRs by ryanodine (100 μM) or dantrolene mimics the effect of thapsigargin (Fig. 4a, Supplementary Fig. 11), whereas blockade of IP_3Rs by xestospongin C has no effect (Supplementary Fig. 12). Thus, a specific defect in RyR-mediated CICR likely underlies the presynaptic impairment in CA3-*PS* cDKO mice.

To determine directly whether Ca^{2+} homeostasis is indeed affected by *PS* inactivation, we performed Ca^{2+} imaging in cultured hippocampal neurons, in which *PS* is acutely inactivated with a lentivirus expressing Cre recombinase. This postnatal culture system circumvents the requirement of presenilins in neurogenesis during embryonic development21, 22 and permits direct measurement of Ca^{2+} concentrations in these neurons. PS expression is abolished in *Cre*-infected (*PS* cDKO) neurons, but their neuronal and synaptic morphology appear normal (Supplementary Fig. 13a, 13c). Similar to CA3-*PS* cDKO mice, presynaptic short-term plasticity measured as paired-pulse ratio is altered in *PS* cDKO hippocampal neurons (Supplementary Fig. 13b), confirming that this preparation recapitulates the presynaptic defect of the *PS*-deficient hippocampus. We then measured somatic $[Ca^{2+}]_i$ changes elicited by depolarization (80 mM KCl), which are contributed by both Ca^{2+} influx through VGCCs and Ca^{2+} efflux from intracellular stores. The amplitude of $[Ca^{2+}]_i$ changes ($\Delta[Ca^{2+}]_i$) elicited by depolarization is reduced in *PS* cDKO neurons (Fig. 4b, Supplementary Fig. 14). Blockade of RyRs with ryanodine (100 μM) in control neurons mimics the effect of *PS* inactivation, whereas ryanodine has no additional effect in *PS* cDKO neurons (Fig. 4b, Supplementary Fig. 14). Thus, blockade of RyRs mimics and occludes the effect of *PS* inactivation on depolarization-induced $[Ca^{2+}]_i$ changes. Blockade of IP_3R with xestospongin C, however, has no effect (Fig. 4b, Supplementary Fig. 14). These results show directly that *PS* inactivation in neurons impairs depolarization-induced Ca^{2+} increases that involve RyR-dependent CICR.

Collectively, our studies demonstrate that loss of PS impairs LTP induction and glutamatergic neurotransmitter release in mature neurons by a presynaptic mechanism (see model in Supplementary Fig. 15). Our pharmacological and imaging studies coupled with

electrophysiological analysis further reveal that a specific impairment in RyR-mediated CICR underlies the presynaptic defects caused by loss of PS. Therefore, the presynaptic function of PS unexpectedly acts, at least in part, on the RyR-mediated Ca^{2+} release from intracellular stores. Finally, our data suggest that short- and long-term plasticity in the hippocampus depend partly on intracellular Ca^{2+} release, which regulates neurotransmitter release.

Prior studies investigating synaptic dysfunction in the pathophysiology of AD have uncovered defects in NMDARs and AMPARs, leading to the notion that postsynaptic impairment may be the early pathogenic change in AD[3, 23, 24]. However, the possibility that impaired presynaptic function may be the primary synaptic defect in AD was largely unexplored. The amyloid precursor protein (APP) and Aβ peptides were reported to be presynaptically localized and were implicated in vesicle recycling[25-27]. Our findings, which distinguish unequivocally between presynaptic and postsynaptic functions of PS, raise the possibility that presynaptic mechanisms play a primary role in AD pathophysiology. This hypothesis is supported by the findings that presenilin is localized to presynaptic terminals (Supplementary Fig. 16), and that APP C-terminal fragments, which are substrates of PS-dependent γ-secretase activity and precursors of Aβ, accumulate in presynaptic terminals of *PS1* cKO mice[28]. Intriguingly, gene products responsible for recessively-inherited familial Parkinson's disease, such as PINK1 and DJ-1, are required for evoked dopamine release from nigrostriatal terminals[29, 30]. These findings suggest that defects in presynaptic neurotransmitter release may represent a general convergent mechanism leading to neurodegeneration.

Methods summary

Electrophysiological analysis

Acute hippocampal slices (400 μm) were prepared as described previously[3]. Synaptic strength was quantified as the initial slope of field potentials recorded with aCSF-filled microelectrodes (1 to 2 MΩ). Intracellular whole-cell recordings were performed using Multiclamp 700B in CA1 or CA3 pyramidal neurons. Data were analyzed using Igor and Clampfit. Experimenters were blind to the genotypes of the mice.

Hippocampal neuronal culture

PS cDKO hippocampal neuronal cultures were derived from *fPS1/fPS1;PS2*$^{-/-}$ pups at postnatal day 1, followed by infection of lentiviral vectors expressing either a functional Cre-GFP or a mutant Cre-GFP fusion protein at 2 DIV for 72 hr. Whole-cell patch recordings from cultured hippocampal neurons at 13-15 DIV were performed at room temperature using a Multiclamp 700B amplifier with pCLAMP acquisition software.

Ca^{2+} imaging

Hippocampal neurons were loaded with Fura-2 AM, and imaged with a Leica DMI6000 Microscope with 40X lens. Imaging processing and data analysis were performed using LAS AF software. High concentrations of potassium were applied using an 8-channel gravity perfusion system.

Methods

Generation of CA1- and CA3- *PS* cDKO mice

CA1- and CA3-*PS* cDKO mice contain homozygous floxed *PS1* alleles, homozygous *PS2*-/- alleles and the *Camk2a-Cre*[7] and *KA1-Cre*[8] transgene, respectively. Since *PS2*-/- mice have no detectable phenotypes[31], it was unnecessary to generate floxed *PS2* mice. For each

cDKO mouse line, *fPS1/fPS1;PS2-/-;Cre* mice were bred with *fPS1/fPS1;PS2-/-* mice to obtain more cDKO mice (*fPS1/fPS1;PS2-/-;Cre*) and *fPS1/fPS1;Cre* were bred with *fPS1/fPS1* to obtain control mice (*fPS1/fPS1*). Introduction of two loxP sites into *PS1* introns 1 and 3 was previously confirmed not to affect transcription, splicing and translation9. The genetic background of these mice was similar in the C57BL6/129 hybrid background with breeding carried out similarly for both groups. All procedures relating to animal care and treatment conformed to the Institutional and NIH guidelines.

In situ hybridization and LacZ staining

In situ hybridization was carried out as previous described using a 260 bp sense or antisense riboprobe specific for *PS1* exons 2 and 3 (Ref. 32). For X-gal staining, *Camk2a-Cre* and *KA1-Cre* transgenic mice were bred to *Rosa26-lacZ* mice, and double transgenic offspring containing both the *Cre* and the *lacZ* transgenes were analyzed.

Field and whole-cell electrophysiological analysis of acute hippocampal slices

All electrophysiological analysis was performed by experimenters who were blind to the genotypes of the mice. Acute hippocampal slices (400 μm) were prepared as described before3. The slices were maintained in a storage chamber containing artificial cerebrospinal fluid (aCSF: 124 mM NaCl, 5 mM KCl, 1.25 mM NaH_2PO_4, 1.3 mM MgCl2, 2.6 mM $CaCl_2$, 26 mM $NaHCO_3$, 10 mM dextrose, pH 7.4, 300-310 mOsm) at 30°C. Stimulation (500 μs) pulses were delivered with a bipolar concentric metal electrode. Synaptic strength was quantified as the initial slope of field potentials recorded with aCSF-filled microelectrodes (1 to 2 MΩ). In LTP recordings, baseline responses were collected every 15 sec with a stimulation intensity that yielded 60% of maximal response. LTP was induced by five episodes of TBS delivered at 0.1 Hz. Each episode contains ten stimulus trains (5 pulses at 100 Hz) delivered at 5 Hz. Average responses (mean ± s.e.m.) are expressed as percentage of pre-TBS baseline response. Synaptic facilitations were measured as the percentage of the fEPSP slope vs. the 1^{st} fEPSP slope at a given stimulus train in individual slices.

Intracellular (whole-cell) recordings were performed using Multiclamp 700B (Molecular device) in CA1 or CA3 pyramidal neurons. Patch pipette (3-5 MΩ) were filled with internal solution consisting of (in mM): 110 Cs-Methanesulfonate, 20 TEA-Cl, 8 KCl, 10 EGTA, 10 Hepes, 5 QX-314, 3 Mg-ATP, 0.3 Na_2GTP (pH = 7.3); 275-285 mOsm. AMPAR responses were recorded in the presence of 50 μM APV and 100 μM picrotoxin to block NMDAR- and GABA type A receptor-mediated responses, respectively. NMDAR responses were recorded in the presence of 10 μM CNQX and 100 μM picrotoxin to block AMPAR- and GABA type A receptor-mediated responses, respectively. For the MK-801 experiment, recordings of NMDAR-mediated EPSC were made every 20s before and during exposure to MK801 (40 μM). The NMDAR-mediated EPSC slope was plotted as a function of stimulus number. Decay curves were normalized to the amplitude of the first EPSC in the presence of MK-801 and were fitted to a single exponential curve to estimate the decay time course. NMDA-mediated EPSC was measured at +40 mV, and was elicited by focal stimulation in the presence of CNQX (10 μM) and picrotoxin (100 μM). To record calcium current through VGCCs, TTX (extracellular, 500 nM) and QX-314 (intracellular, 5 mM) were used to block sodium current; Cs^+ (intracellular, 110 mM) and TEA (intracellular, 20 mM) were used to block potassium current. To measure the synaptic facilitation, values of the fEPSP slope (2^{nd}, 3^{rd} …10^{th} responses in a 20-pulse stimulus train) were normalized to the slope of the 1^{st} fEPSP of the stimulus train. Data were analyzed using Igor (Wavemetrics) and Clampfit (Molecular device).

PS cDKO hippocampal neuronal cultures

To circumvent the requirement of PS in neurogenesis during embryonic development21, 22, we established *PS* cDKO hippocampal neuronal cultures derived from *fPS1/fPS1;PS2*$^{-/-}$ newborn pups, followed by infection of lentiviral vectors expressing either a functional Cre-GFP or a mutant Cre-GFP fusion protein. Hippocampi from *fPS1/fPS1;PS2*$^{-/-}$ pups were dissected and treated with 0.25% trypsin at 37°C for 20 min. Cells were plated at a density of 65,000 cells/cm^2 on poly-D-lysine-coated 35 mm dishes (Costar). Cultures were infected with lentiviruses (300 μl condition medium per well in a 24-well plate) expressing at 2 DIV for 72 hr. Infected neurons were cultured until 13-15 DIV for further biochemical, morphological, electrophysiological and imaging analyses. Lentiviruses were produced by transfecting human embryonic kidney HEK293 cells (CRL-11268, ATCC) with the respective pFUGW vectors and two helper plasmids (pVSVg and pCMVΔ8.9) using FUGENE 6 (Roche), as previously described33. Condition medium containing viruses were harvested 48 hr after transfection, and were spun (800g for 5 min) to remove HEK cell debris before adding to the neuronal culture.

Morphological analysis of postnatal hippocampal cultures

Cultured neurons at 14 DIV were fixed with methanol (-20°C). Fixed cultures were then incubated with primary antibodies against synaptophysin (monoclonal; 1:200; Sigma) and microtubule-activated protein 2 (MAP2; polyclonal; 1:250; Sigma) for 1 hr at room temperature. After rinsing three times with PBBS, the neurons were incubated with fluorescent secondary antibodies for 30 min. After washing, cultures were mounted with Vectashield mounting medium (H-1000, Vector labs). Confocal microscopic analysis was performed on a Zeiss LSM 510 microscope. Identical acquisition settings were applied to all samples of the experiment. Images of neurons were collected with 40x oil-immersion objective lens. Images were analyzed in a genotype blind manner using the NIH Image/ Image J program.

Whole-cell electrophysiological analysis of postnatal hippocampal cultures

Whole-cell patch recordings from cultured hippocampal neurons at 13-15 DIV were performed at room temperature using a Multiclamp 700B amplifier (Molecular device) with pCLAMP acquisition software. Synaptic transmission was elicited with a concentric focal stimulus electrode, and EPSCs were recorded with a patch electrode (3-5 MΩ) in whole-cell recording mode and filtered at 2 kHz. Pipette solution contained (in mM): 136.5 K-gluconate, 0.2 EGTA, 10 HEPES, 9 NaCl, 17.5 KCl, 5 QX-314, 4 Mg-ATP, and 0.3 Na-GTP (adjusted to pH 7.4 with KOH). The extracellular solution was a HEPES-buffered saline containing (in mM): 145 NaCl, 3 KCl, 10 HEPES, 2 $CaCl_2$, 1 $MgCl_2$, 8 dextrose (pH 7.2).

Calcium imaging analysis

Hippocampal neurons were loaded with Fura-2 AM (5 μM, 45 min at 37°C) (Molecular probes), and imaged with a Leica DMI6000 Microscope with 40X lens (numerical aperture 0.75). The method and parameters for in vitro calibration (invitrogen calibration kit, F-6774) were as described previously34. Imaging processing and data analysis were performed using LAS AF software (Leica). High concentrations of potassium were applied using an 8-channel gravity perfusion system (ALA Scientific Instrument).

Subcellular fractionation analysis

For enrichment of synaptic vesicle (presynaptic) proteins, four adult cortices (3-month-old) were homogenized with a Dounce teflon homogenizer in ice-cold buffer containing 0.32M sucrose, 4 mM HEPES pH 7.3, and protease and phosphatase inhibitor cocktails. For the P2

fraction, crude homogenates were centrifuged at 800g twice to remove debris; the supernatant were centrifuged at 9200g; and the pellet was resuspended in 0.32M sucrose buffer. For the LP1 fraction, P2 synaptosomes were centrifuged at 10, 200g, resuspended in 0.32M sucrose buffer and hypotonically lysed in 9 volumes of water. The lysate were centrifuged at 25,000g, and the pellet was resuspended in buffer containing 1% NP-40 to produce LP1. For the LP2 fraction, the supernatant from the LP1 purification step was centrifuged at 165,000g, and the pellet was resuspended in buffer containing 1% NP-40.

Supplementary Material

Refer to Web version on PubMed Central for supplementary material.

Acknowledgments

We would like to thank Kazu Nakazawa and Susumu Tonegawa for KA1-Cre transgenic mice, Ray Kelleher for discussions and comments, and Xiaoyan Zou for technical assistance. This work was supported by a grant from the National Institutes of Health (R01NS041783 to JS).

References

1. Hardy J, Selkoe DJ. The amyloid hypothesis of Alzheimer's disease: progress and problems on the road to therapeutics. Science. 2002; 297:353–356. [PubMed: 12130773]
2. Hsia AY, et al. Plaque-independent disruption of neural circuits in Alzheimer's disease mouse models. Proc. Natl. Acad. Sci. USA. 1999; 96:3228–3233. [PubMed: 10077666]
3. Saura CA, et al. Loss of presenilin function causes impairments of memory and synaptic plasticity followed by age-dependent neurodegeneration. Neuron. 2004; 42:23–36. [PubMed: 15066262]
4. Selkoe DJ. Alzheimer's disease is a synaptic failure. Science. 2002; 298:789–791. [PubMed: 12399581]
5. Shen J, Kelleher RJ 3rd. The presenilin hypothesis of Alzheimer's disease: evidence for a loss-of-function pathogenic mechanism. Proc. Natl. Acad. Sci. USA. 2007; 104:403–409. [PubMed: 17197420]
6. Feng R, et al. Forebrain degeneration and ventricle enlargement caused by double knockout of Alzheimer's presenilin-1 and presenilin-2. Proc. Natl. Acad. Sci. USA. 2004; 101:8162–8167. [PubMed: 15148382]
7. Zakharenko SS, et al. Presynaptic BDNF required for a presynaptic but not postsynaptic component of LTP at hippocampal CA1-CA3 synapses. Neuron. 2003; 39:975–990. [PubMed: 12971897]
8. Nakazawa K, et al. Requirement for hippocampal CA3 NMDA receptors in associative memory recall. Science. 2002; 297:211–218. [PubMed: 12040087]
9. Yu H, et al. APP processing and synaptic plasticity in presenilin-1 conditional knockout mice. Neuron. 2001; 31:713–726. [PubMed: 11567612]
10. Hessler NA, Shirke AM, Malinow R. The probability of transmitter release at a mammalian central synapse. Nature. 1993; 366:569–572. [PubMed: 7902955]
11. Rosenmund C, Clements JD, Westbrook GL. Nonuniform probability of glutamate release at a hippocampal synapse. Science. 1993; 262:754–757. [PubMed: 7901909]
12. Emptage NJ, Reid CA, Fine A. Calcium stores in hippocampal synaptic boutons mediate short-term plasticity, store-operated Ca^{2+} entry, and spontaneous transmitter release. Neuron. 2001; 29:197–208. [PubMed: 11182091]
13. Chan SL, Mayne M, Holden CP, Geiger JD, Mattson MP. Presenilin-1 mutations increase levels of ryanodine receptors and calcium release in PC12 cells and cortical neurons. J. Biol. Chem. 2000; 275:18195–18200. [PubMed: 10764737]
14. Green KN, et al. SERCA pump activity is physiologically regulated by presenilin and regulates amyloid beta production. J. Cell Biol. 2008; 181:1107–1116. [PubMed: 18591429]
15. Stutzmann GE, Caccamo A, LaFerla FM, Parker I. Dysregulated IP3 signaling in cortical neurons of knock-in mice expressing an Alzheimer's-linked mutation in presenilin1 results in exaggerated

Ca^{2+} signals and altered membrane excitability. J. Neurosci. 2004; 24:508–513. [PubMed: 14724250]

16. Tu H, et al. Presenilins form ER Ca^{2+} leak channels, a function disrupted by familial Alzheimer's disease-linked mutations. Cell. 2006; 126:981–993. [PubMed: 16959576]
17. Treiman M, Caspersen C, Christensen SB. A tool coming of age: thapsigargin as an inhibitor of sarco-endoplasmic reticulum $Ca^{(2+)}$-ATPases. Trends Pharmacol. Sci. 1998; 19:131–135. [PubMed: 9612087]
18. Gafni J, et al. Xestospongins: potent membrane permeable blockers of the inositol 1,4,5-trisphosphate receptor. Neuron. 1997; 19:723–733. [PubMed: 9331361]
19. Meissner G. Ryanodine activation and inhibition of the Ca^{2+} release channel of sarcoplasmic reticulum. J. Biol. Chem. 1986; 261:6300–6306. [PubMed: 2422165]
20. Stutzmann GE, et al. Enhanced ryanodine receptor recruitment contributes to Ca^{2+} disruptions in young, adult, and aged Alzheimer's disease mice. J. Neurosci. 2006; 26:5180–5189. [PubMed: 16687509]
21. Handler M, Yang X, Shen J. Presenilin-1 regulates neuronal differentiation during neurogenesis. Development. 2000; 127:2593–2606. [PubMed: 10821758]
22. Shen J, et al. Skeletal and CNS defects in Presenilin-1-deficient mice. Cell. 1997; 89:629–639. [PubMed: 9160754]
23. Kamenetz F, et al. APP processing and synaptic function. Neuron. 2003; 37:925–937. [PubMed: 12670422]
24. Snyder EM, et al. Regulation of NMDA receptor trafficking by amyloid-beta. Nat. Neurosci. 2005; 8:1051–1058. [PubMed: 16025111]
25. Buxbaum JD, et al. Alzheimer amyloid protein precursor in the rat hippocampus: transport and processing through the perforant path. J. Neurosci. 1998; 18:9629–9637. [PubMed: 9822724]
26. Lazarov O, Lee M, Peterson DA, Sisodia SS. Evidence that synaptically released beta-amyloid accumulates as extracellular deposits in the hippocampus of transgenic mice. J. Neurosci. 2002; 22:9785–9793. [PubMed: 12427834]
27. Yao PJ, Coleman PD. Reduced O-glycosylated clathrin assembly protein AP180: implication for synaptic vesicle recycling dysfunction in Alzheimer's disease. Neurosci. Lett. 1998; 252:33–36. [PubMed: 9756352]
28. Saura CA, et al. Conditional inactivation of presenilin 1 prevents amyloid accumulation and temporarily rescues contextual and spatial working memory impairments in amyloid precursor protein transgenic mice. J. Neurosci. 2005; 25:6755–6764. [PubMed: 16033885]
29. Goldberg MS, et al. Nigrostriatal dopaminergic deficits and hypokinesia caused by inactivation of the familial Parkinsonism-linked gene DJ-1. Neuron. 2005; 45:489–496. [PubMed: 15721235]
30. Kitada T, et al. Impaired dopamine release and synaptic plasticity in the striatum of PINK1-deficient mice. Proc. Natl. Acad. Sci. USA. 2007; 104:11441–11446. [PubMed: 17563363]
31. Steiner H, et al. A loss of function mutation of presenilin-2 interferes with amyloid beta-peptide production and notch signaling. J. Biol. Chem. 1999; 274:28669–28673. [PubMed: 10497236]
32. Wines-Samuelson M, Handler M, Shen J. Role of presenilin-1 in cortical lamination and survival of Cajal-Retzius neurons. Dev. Biol. 2005; 277:332–346. [PubMed: 15617678]
33. Watanabe H, et al. Indirect regulation of presenilins in CREB-mediated transcription. J. Biol. Chem. 2009; 284:13705–13713. [PubMed: 19289467]
34. Zhang C, Zhou Z. $Ca^{(2+)}$-independent but voltage-dependent secretion in mammalian dorsal root ganglion neurons. Nat. Neurosci. 2002; 5:425–430. [PubMed: 11953753]

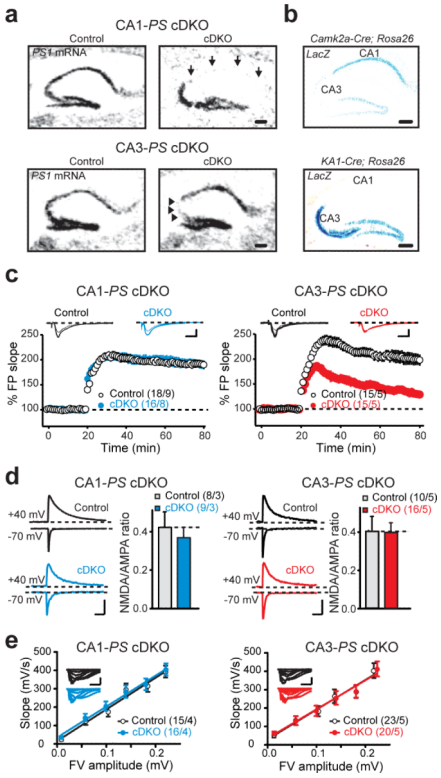

Figure 1. Impaired LTP in CA3- but not CA1- *PS* cDKO mice

a. *In situ* hybridization shows loss of *PS1* mRNAs in CA1 (arrows) and CA3 (arrowheads) neurons in CA1- and CA3-*PS* cDKO mice, respectively. Scale bar: 200 μm. **b**. X-gal staining shows absence of Cre-mediated recombination in CA3 and CA1 neurons of *Camk2a-Cre; Rosa26-lacZ* and *KA1-Cre*; *Rosa26-lacZ* mice, respectively. Scale bar: 200 μm. **c**. TBS-induced LTP in CA1-*PS* cDKO (filled blue circles) and CA3-*PS* cDKO (filled red circles) compared to their controls (open circles). Representative traces before (thin) and after (thick) LTP induction are shown. Superimposed traces are averages of four consecutive responses 1 min before and 60 min after TBS. Scale bar: 10 ms, 1 mV. **d**. Normal ratio of NMDAR- to AMPAR- responses in CA3- and CA1-*PS* cDKO mice. Scale bar: 200 ms, 200 pA. **e**. NMDAR-mediated input/output curves. Scale bar: 40 ms, 1 mV. All data represent mean ± s.e.m. The number of hippocampal neurons or slices (left) and mice (right) used in each experiment is indicated in parenthesis.

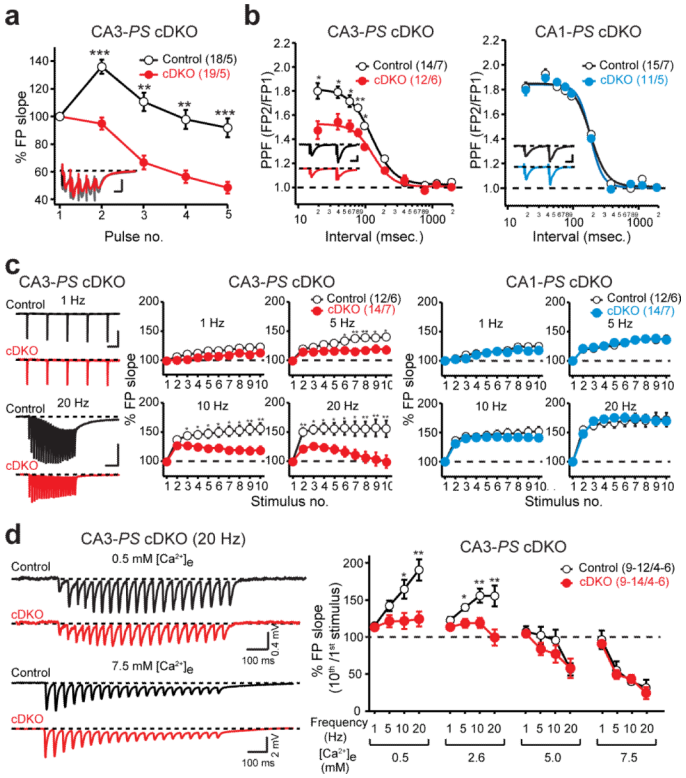

Figure 2. Presynaptic defects in CA3- but not CA1-*PS* cDKO mice

a. Reduced facilitation of fEPSP slope during single TBS in CA3-*PS* cDKO mice. Inset shows representative traces of field responses during single TBS stimulus train. Scale bar: 10 ms, 2 mV. **b**. Paired-pulse facilitation in CA3- and CA1-*PS* cDKO mice. Scale bars in insets: 10 ms, 0.5 mV. **c**. Synaptic facilitation elicited by stimulus trains of indicated frequencies in CA3- and CA1-*PS* cDKO mice. Scale bars: top, 2 mV, 500 ms; bottom, 2 mV, 250 ms. **d**. Calcium dependence of frequency facilitation defects in CA3-*PS* cDKO mice. Scale bars: top, 0.4 mV, 100 ms; bottom, 2 mV, 100 ms. All data represent mean ± s.e.m. *p < 0.05; **p < 0.01; ***p < 0.001. The number of slices (left) and mice (right) used in each experiment is indicated in parenthesis.

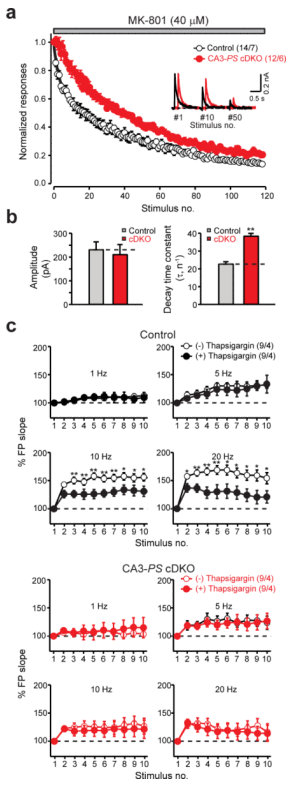

Figure 3. Presynaptic PS regulates glutamate release via intracellular Ca^{2+} stores

a. Reduced decay rate of NMDAR-mediated responses in the presence of MK-801 in CA3-*PS* cDKO mice. **b**. Amplitude of the first NMDAR-mediated response (left) and decay time constant (fitted to a single exponential curve) of the NMDAR-mediated EPSC slope in the presence of MK-801 (right). Representative traces of EPSCs after the 1st, 10th and 50th stimulus are shown in the inset. **c**. Effects of thapsigargin treatment on synaptic facilitation in control and CA3-*PS* cDKO slices. All data represent mean ± s.e.m. *p < 0.05; **p < 0.01. The number of slices or neurons (left) and mice (right) used in each experiment is indicated in parenthesis.

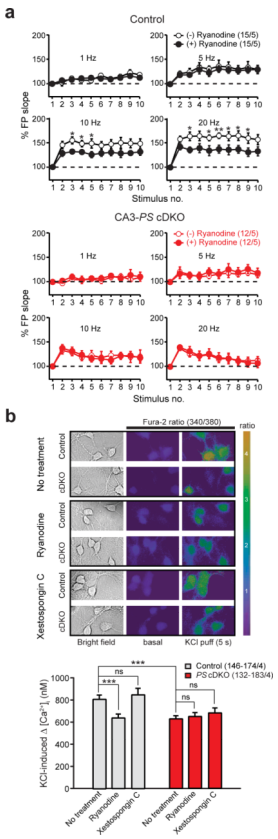

Figure 4. Blockade of RyRs mimics and occludes the defects in synaptic facilitation and calcium homeostasis in CA3-*PS* cDKO hippocampal slices and cultured *PS* cDKO hippocampal neurons

a. Effect of ryanodine (100 μM) treatment on synaptic facilitation in control and CA3-*PS* cDKO mice. **b**. Effect of ryanodine (100 μM) or xestospongin C (1 μM) treatment on depolarization-induced $[Ca^{2+}]_i$ increases in cultured hippocampal neurons. Representative calcium images (top) show high potassium (80 mM)-induced Ca^{2+} responses in control and *PS* cDKO neurons. All data represent mean ± s.e.m. *p < 0.05; **p < 0.01. The number of slices or neurons (left) and mice or experiments (right) involved is indicated in parenthesis.